Submitted for the proceedings of the Sentinel-3for Science Workshop held in
Venice - Lido, Italy, 2-5 June 2015, ESA Special Publication SP – 7 34

CLOUD AND CLOUD SHADOW IDENTIFICATION FOR MERIS AND SENTINEL-3/OLCI

Nicholas Pringle, Quinten Vanhellemont and Kevin Ruddick.

Operational Directorate Natural Environment.
Royal Belgian Institute for Natural Science, Gulledelle 100, 1200. Brussels
npringle@naturalsciences.be

ABSTRACT

Ocean colour remote sensing has become a well-established method for the monitoring of coastal waters. The MERIS chlorophyll product for turbid waters (algal_2) and the total suspended matter product (tsm) have been used in applications such as algal bloom detection, eutrophication monitoring, and coastal sediment transport. These MERIS L2 products are sometimes contaminated by cloud shadow pixels and the same problems are likely to occur in Sentinel-3. In order to avoid erroneous data passing quality control and being used in applications, an automated method for detecting and removing cloud and cloud shadow pixels is needed. With this in mind, we highlight the problems with MERIS in the past and show some results from applying detection methods to Landsat-8 data with the objective of using these methods for Sentinel-2 and -3 in the future.

1. Introduction

As a follow up to the MERIS, MODIS and SeaWiFS missions, the Sentinel-3 satellite with its Ocean and Land Color Instrument (OLCI) will supply operational services for land, coastal and marine environmental monitoring. OLCI will provide multispectral medium resolution imagery, with high spectral and temporal resolution (1-3 days).

OLCI has been designed with strong heritage from the MERIS mission. In this context it is important to identify the shortcomings of the MERIS products and see how these can be avoided with OLCI. A problem common to all earth observation satellites is the presence of clouds and clouds shadows (Fig. 1).

The MERIS Case 2 chlorophyll products [1] have been used for applications in turbid waters such as the detection and timing of algal blooms [2] and for the validation of an ecosystem model [3]. The MERIS products have been very useful but it is important to note that the MERIS L2 chlorophyll and tsm products are sometimes contaminated with unmasked cloud shadow pixels in the third reprocessing (R3) and prior processor versions. This is still the case when applying the PCD_17 and PCD_16 flags for algal_2 and tsm respectively as seen in Fig. 2 and Fig. 3.

When using the R3/PCD_1_13 flag to flag for bad pixels (Fig. 4) we remove many of the cloud shadow pixels as well as many other pixels. Additionally there are some cloud shadow pixels especially in turbid waters that are not flagged as cloud shadow pixels and therefore give incorrect data. Thus, using the PCD_1_13 flag is not ideal.

We also processed the MERIS data with SeaDAS/l2gen (version 7.2) with the extended standard approach[4], [5] for atmospheric correction. Using SeaDAS processing we see similar problems. Using the LOWLW flag (low reflectance at 555nm) we see in Fig. 5a and b that some cloud shadows are masked in clear waters but that cloud shadows are not masked in more turbid waters.

A methodology originally developed for the Landsat-8 Operational Land Imager (OLI) is described here as a basis for a future OLCI algorithm for cloud and cloud shadow detection.

2. Data and Methods

Landsat L1 data in GeoTIFF format obtained from USGS is used. Digital Numbers from the Landsat L1 files are converted to Top of Atmosphere (TOA) reflectance and then further processed into Rayleigh corrected (Rc) and marine reflectance (rhow) using ACOLITE [6], [7]. Additionally, brightness temperature is calculated from the Landsat-8 Thermal Infrared Sensor which provides thermal bands at 100 meters resolution which are resampled to 30 meters to match multispectral bands.

A cloud and cloud shadow identification method is adapted from the Fmask algorithm of Zhu and Woodcock [8], [9]. A number of steps are used to test for cloud contamination of pixels (Fig. 6). Two passes are used to identify cloud pixels.

The first pass uses the spectral information from the TOA and Rc data. The basic test (eq. 1) sets thresholds for the normalized difference vegetation index (NDVI) and normalized difference snow index NDSI at less than 0.8, the SWIR reflectance 2201nm at greater than 0.0215 and the Brightness Temperature at less than

27deg C. The whiteness test (eq. 3) flags pixels with a whiteness greater than 0.7. The Haze Optimized Transform (HOT) Test (eq. 4) is used to flag pixels where (blue – red/2) is greater than 0. The cirrus test (eq. 6) is used to identify cirrus clouds as pixels with a TOA reflectance at 1373nm of greater than 0.01. The potential cloud pixels (PCP) are then flagged using the eq. 8.

The second pass uses spatial information from the scene. Temperature probability (eq. 10), brightness probability (eq. 11) and variability probability (eq. 16) are calculated, the method being slightly different over land and water [8]. Water cloud probability (eq. 12) and land cloud probability (eq. 17) are calculated from these. This removes many of the inaccurately assigned cloud pixels.

To identify cloud shadow, the sun zenith and azimuth angles are used to estimate the region where pixels may fall in the shadow of the cloud. An estimation of cloud height for each cloud object, or a maximum cloud height of 12000m may be used to determine the cloud shadow region. Low reflectance in the visible, NIR and SWIR bands are used with the geometric information (projection of cloud object) to flag possible cloud shadow pixels. Thus, pixels with low reflectance that also fall within what is estimated to be the cloud shadow are flagged as cloud shadow pixels.

Mountain shadows could similarly be identified by using a digital elevation model (DEM). A mountain shadow can be predicted by using the sun zenith, sun azimuth angles and the mountain height and in this way mountain shadow falling on water surfaces can be flagged as mountain shadow.

3. Results

An example from the Belgian Coastal zone in the Southern North Sea (Fig. 7) shows successful pixel identification in the Landsat Scene LC81990242013280LGN00 for land, water, cloud and cloud shadow.

Fig. 7 shows an RGB image, cloud pixel identification, cloud shadow identification and a composite of cloud and cloud shadow pixel on a smaller subset. Although most cloud shadow pixels are identified it appears as if the cloud shadow flag would benefit from a one to three pixel buffer.

In this scene, some water pixels with a low reflectance are masked as cloud shadow pixels even though it appears as if they are not. This is due to the proximity of some clouds to water with a relatively low reflectance to the rest of the water. In turbid water it may be easier to identify cloud shadow using low reflectance values in the visible bands.

Validation is done subjectively, currently the most effective way of assessing cloud and cloud shadow masks. The procedure has been repeated for other relatively cloud free scenes in Belgian waters with similar results.

4. Discussion

The 21 bands in Sentinel-3 OLCI are based on the 15 bands from MERIS (Table. 1). Due to differences in their respective objectives, there are differences between the bands available in Landsat-8 (Table 3) and Sentinel-3 OLCI. Important difference for cloud and cloud shadow identification include the absence of a cirrus band, the thermal infrared (TIR) bands (which is on Landsat-8 TIRS) and short wave infrared bands (SWIR). This provides some limitations on cloud and cloud shadow identification.

The absence of these bands mean that calculating the brightness temperature, using a SWIR threshold and identifying cirrus clouds will not be possible using OLCI alone. Information from the Sentinel-3 SLSTR bands might be used to supplement the information from the OLCI bands.

The whiteness test [10] and the Haze Optimized Transform test [11] can still be used with the bands available from Sentinel-3 OLCI for the first pass of the cloud identification method. The second pass would not be possible with OLCI bands alone as it relies on the brightness temperature or cirrus probability [8].

The Sentinel-3 SLSTR sensor (Table. 2) will have the bands that OLCI requires albeit at a different resolution than the OLCI bands, with 500m for the solar reflectance band and 1km for the thermal bands. In addition to cloud and cloud shadow identification, the Sentinel-3 SLSTR sensor could be useful for atmospheric correction and pixel identification provided that co-location and intercalibration are good (Ruddick and Vanhellemont, 2014, this issue).

Sentinel-3 OLCI will have an oxygen absorption band and a maximum water vapor absorption band which will make it useful for identifying cloud pixels and estimating cloud height. Cloud height is an important component in calculating the geometry for the cloud shadow identification. The band at 1020nm will also be useful for cloud and snow differentiation. A combination of good cloud pixel identification and cloud height estimation will be very useful for

calculating the cloud shadow mask based on sun and sensor geometry.

5. Conclusion

MERIS L2 products are sometimes contaminated with unmasked cloud shadow pixels, particularly for turbid waters. This will likely be a problem with Sentinel-3 L2 products.

Using Landsat-8, it is shown that it is possible to automatically mask cloud shadow pixels. The methods used to identify cloud and cloud shadow pixels can be adapted to Sentinel-3 as well as Sentinel-2.

With the OLCI oxygen absorption and water vapour bands, as well as the bands available on the SLSTR sensor, it should be possible to create a cloud and cloud shadow flag to avoid pixel contamination in Sentinel-3 products.

6. Acknowledgements

This research was performed for the HIGHROC project. The HIGHROC project is funded by the European Community's Seventh Framework Programme (FP7/2007-2015) under grant agreement n° 606797. We thank NASA USGS for the Landsat-8 data. We thank ESA for the MERIS data.

7. Equations

$$basic\ test = \rho_{rc}^{2201} > 0.0215\ and\ BT < 27℃\ and\ NDSI < 0.8\ and\ NDVI < 0.8 \quad (1)$$

$$MeanVis = \frac{\rho_{toa}^{483} + \rho_{toa}^{581} + \rho_{toa}^{655}}{3} \quad (2)$$

$$Whiteness\ index = \sum_{i=483,561,655} \left| \frac{(\rho^i - MeanVis)}{MeanVis} \right| < 0.7 \quad (3)$$

$$HOT\ test = \rho_{toa}^{483} - 0.5 * \rho_{toa}^{561} - 0.08 > 0 \quad (4)$$

$$nir/swir\ test = \left(\frac{\rho_{rc}^{865}}{\rho_{rc}^{1609}} > 0.75 \right) \quad (5)$$

$$cirrus\ test = cirrus\ band > 0.04 \quad (6)$$

$$clear - sky\ water = water\ test\ (True)\ and\ \rho_{rc}^{1609} < 0.03 \quad (7)$$

$$PCP = \begin{pmatrix} Basic\ Test \\ AND \\ Whiteness\ Test \\ AND \\ HOT\ Test \\ AND \\ \frac{SWIR}{NIR}\ Test \end{pmatrix} OR\ Cirrus\ Test \quad (8)$$

$$T_{water} = 82.5th\ percentile\ of\ clear - sky\ water\ pixels\ BT \quad (9)$$

$$wTemperature_{Prob} = (T_{water} - BT)/4 \quad (10)$$

$$Brightness_{prob} = \min(\rho_{rc}^{1609}, 0.11)\ /0.11 \quad (11)$$

$$wCloud_{prob} = wTemperature_{prob} * Brightness_{prob} \quad (12)$$

$$Clear - sky\ land = PCP(false) and\ water\ Test\ (false) \quad (13)$$

$$(T_{low}, T_{high}) = (17.5, 82.5) percetile\ of\ Clear - sky\ land\ pixels' BT \quad (14)$$

$$lTemperature_{prob} = (T_{high} + 4 - BT)/(\ T_{low} + 4 - (T_{low} - 4)) \quad (15)$$

$$Variability_{prob} = 1 - \max(abs(NDVI), abs(NDSI), Whiteness) \quad (16)$$

$$lCloud_{prob} = lTemperature_{prob} * Variability_{prob} \quad (17)$$

$$LandThreshold = 82.5\ percetinle\ of\ lCloud_{prob(Clear-sky\ land\ pixels)} + 0.2 \quad (18)$$

$$PCP\ and\ Water\ and\ wCloud_{prob} > 0.5$$
$$PCP\ and\ !Water\ and\ lCloud_{prob} > LandThreshold$$
$$lCloud_{prob} > 0.99\ and\ !Water$$
$$BT < T_{low} - 35 \quad (19)$$

Where

$$NDSI = \frac{(\rho_{rc}^{561} - \rho_{rc}^{1609})}{(\rho_{rc}^{561} + \rho_{rc}^{1609})}$$

$$NDVI = \frac{(\rho_{rc}^{655} - \rho_{rc}^{561})}{(\rho_{rc}^{655} + \rho_{rc}^{561})}$$

8. References

[1] R. Doerffer and H. Schiller, "The MERIS Case 2 water algorithm," *Int. J. Remote Sens.*, vol. 28, no. 3–4, pp. 517–535, Feb. 2007.

[2] Y.-J. Park, K. Ruddick, and G. Lacroix, "Detection of algal blooms in European waters based on satellite chlorophyll data from MERIS and MODIS," *Int. J. Remote Sens.*, vol. 31, no. 24, pp. 6567–6583, Dec. 2010.

[3] G. Lacroix, K. Ruddick, Y. Park, N. Gypens, and C. Lancelot, "Validation of the 3D biogeochemical model MIRO&CO with field nutrient and phytoplankton data and MERIS-derived surface chlorophyll a images," *J. Mar. Syst.*, vol. 64, no. 1–4, pp. 66–88, Jan. 2007.

[4] H. R. Gordon and M. Wang, "Retrieval of water-leaving radiance and aerosol optical thickness over the oceans with SeaWiFS: a preliminary algorithm," *Appl. Opt.*, vol. 33, no. 3, p. 443, Jan. 1994.

[5] S. W. Bailey, B. A. Franz, and P. J. Werdell, "Estimation of near-infrared water-leaving reflectance for satellite ocean color data processing," *Opt. Express*, vol. 18, no. 7, pp. 7521–7527, Mar. 2010.

[6] Q. Vanhellemont and K. Ruddick, "Turbid wakes associated with offshore wind turbines observed with Landsat 8," *Remote Sens. Environ.*, vol. 145, pp. 105–115, Apr. 2014.

[7] Q. Vanhellemont and K. Ruddick, "Advantages of high quality SWIR bands for ocean colour processing: Examples from Landsat-8," *Remote Sens. Environ.*, vol. 161, pp. 89–106, May 2015.

[8] Z. Zhu and C. E. Woodcock, "Object-based cloud and cloud shadow detection in Landsat imagery," *Remote Sens. Environ.*, vol. 118, pp. 83–94, Mar. 2012.

[9] Z. Zhu, S. Wang, and C. E. Woodcock, "Improvement and expansion of the Fmask algorithm: cloud, cloud shadow, and snow detection for Landsats 4–7, 8, and Sentinel 2 images," *Remote Sens. Environ.*, vol. 159, pp. 269–277, Mar. 2015.

[10] L. Gomez-Chova, G. Camps-Valls, J. Calpe-Maravilla, L. Guanter, and J. Moreno, "Cloud-Screening Algorithm for ENVISAT/MERIS Multispectral Images," *IEEE Trans. Geosci. Remote Sens.*, vol. 45, no. 12, pp. 4105–4118, Dec. 2007.

[11] Y. Zhang, B. Guindon, and J. Cihlar, "An image transform to characterize and compensate for spatial variations in thin cloud contamination of Landsat images," *Remote Sens. Environ.*, vol. 82, no. 2–3, pp. 173–187, Oct. 2002.

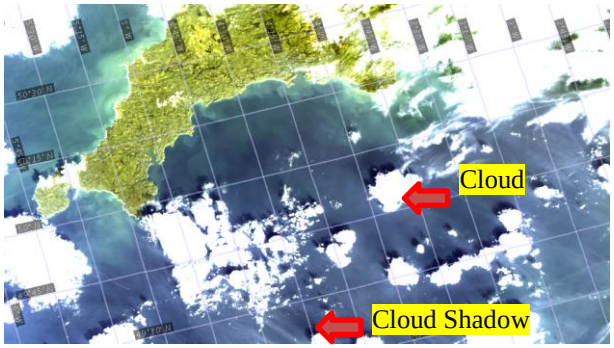

Figure 1: MERIS (2013-01-16) RGB image (MERIS L2 tristimulus with adjusted histograms) for the western English Channel. Cloud and cloud shadow are annotated in the image with arrows.

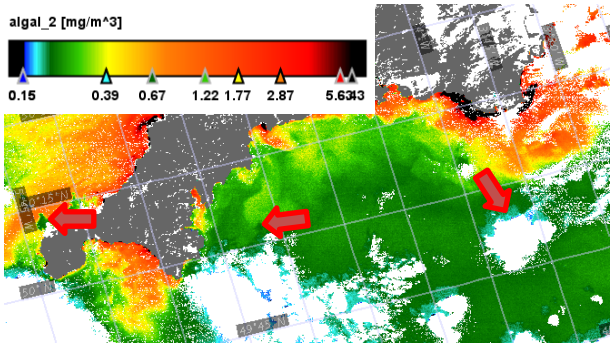

Figure 2: Algal 2 product from MERIS (2003-01-16) MEGS 8.0 processing with the PCD_17 confidence flag. Arrows identify examples of cloud shadows that have not been flagged.

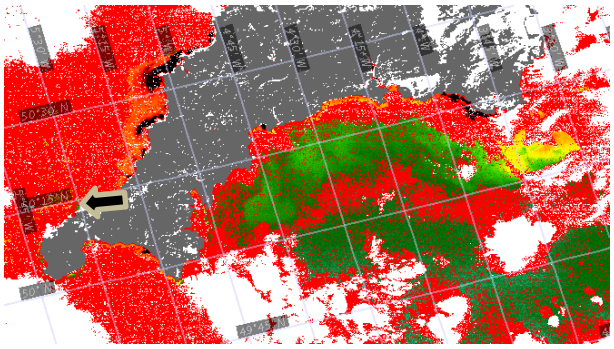

Figure 4: Total Suspended Matter product from MERIS (2003-01-16) MEGS 8.0 processing with the PCD_1_13 confidence flag (red). Arrow shows example of cloud shadow not masked flagged.

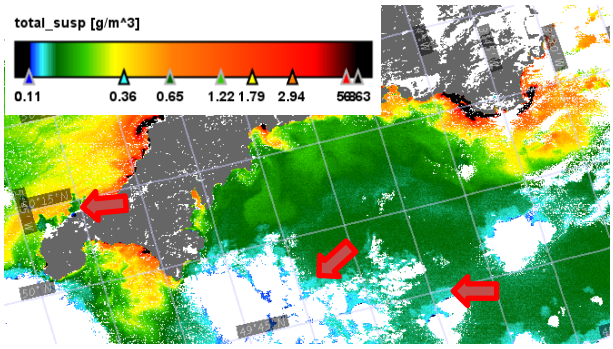

Figure 3: Total Suspended Matter product from MERIS (2003-01-16) MEGS 8.0 processing with the PCD_16 confidence flag. Arrows identify examples of cloud shadows that have not been flagged.

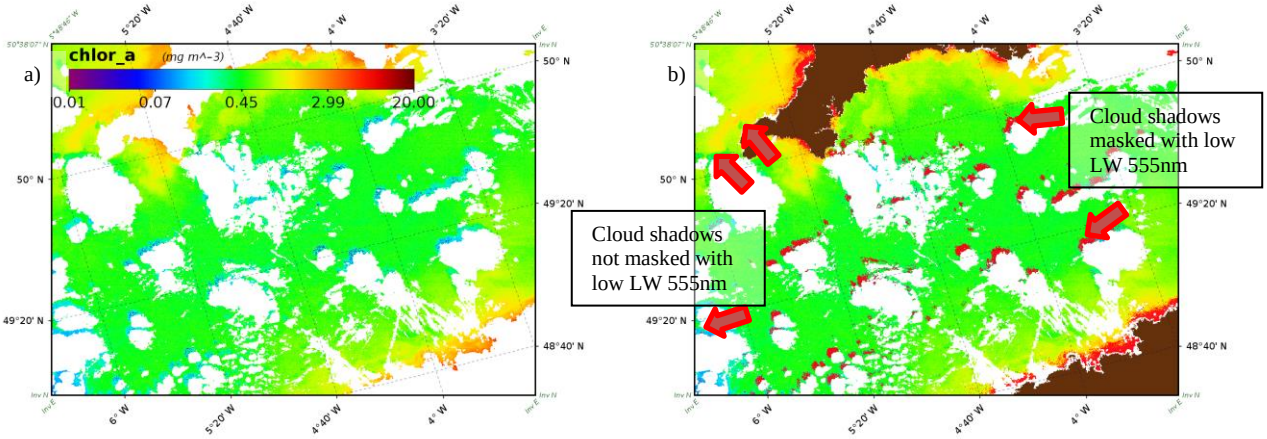

Figure 5: MERIS (2003-01-16) Chlorophyll-a processed with SeaDAS (a) and Chlorophyll-a with a LOWLW mask in red (b). Annotation in the zoomed subset identifies cloud shadow pixels that have been masked in less turbid waters and cloud shadow pixels that have not been masked in turbid water.

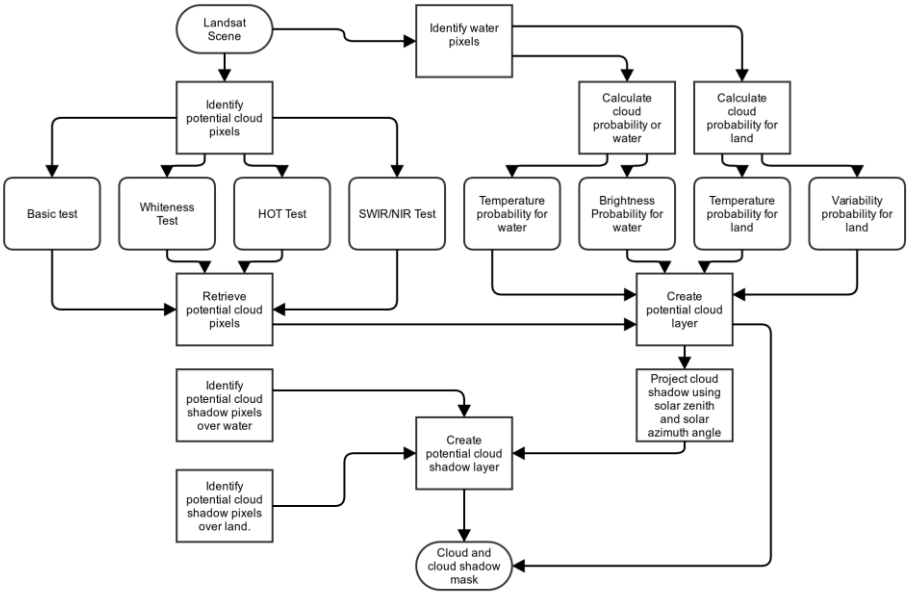

Figure 6: Schematic of workflow used to identify cloud and cloud shadow pixels in Landsat-8 imagery.

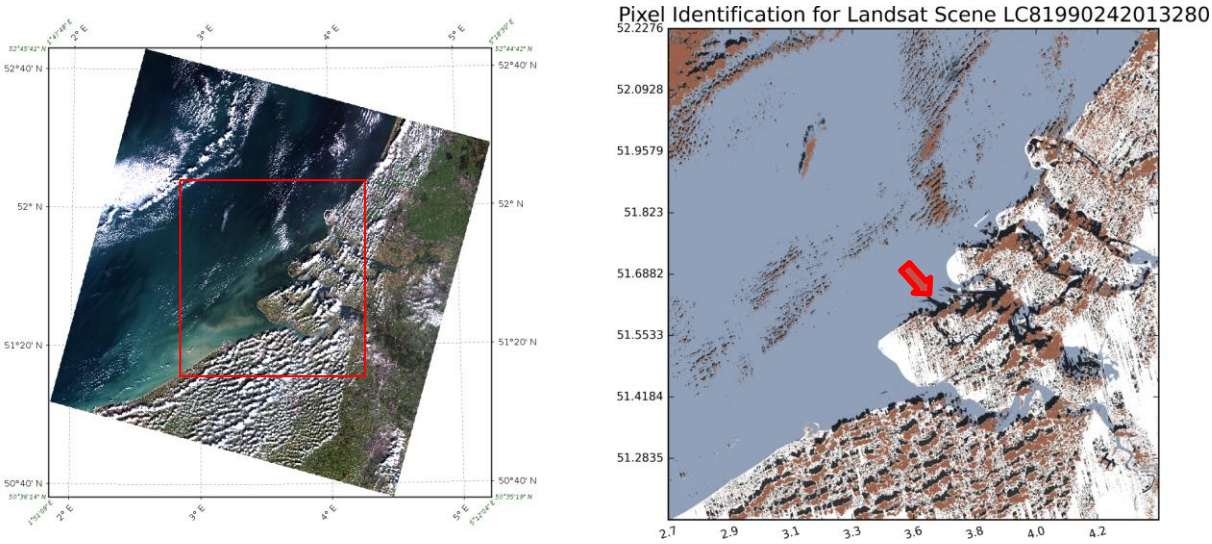

Figure 7: Subset of land (white), water (blue-grey), cloud (orange) and cloud shadow (black) identification (left) and full scene RGB image (right) for Landsat-8 scene LC81990242013280LGN00. Incorrectly flagged cloud shadow shown with red arrow.

Table 1: Band characteristics of the Sentinel-3 Ocean and Land Colour Instrument (OLCI). Rows highlighted in blue show bands that match with Landsat-8/OLI.

Band	λ centre nm	Width Nm
Oa1	400	15
Oa2	412.5	10
Oa3	442.5	10
Oa4	490	10
Oa5	510	10
Oa6	560	10
Oa7	620	10
Oa8	665	10
Oa9	673.75	7.5
Oa10	681.25	7.5
Oa11	708.75	10
Oa12	753.75	7.5
Oa13	761.25	2.5
Oa14	764.375	3.75
Oa15	767.5	2.5
Oa16	778.75	15
Oa17	865	20
Oa18	885	10
Oa19	900	10
Oa20	940	20
Oa21	1020	40

Table 2: Band characteristics of the Sentinel-3 Sea and Land Surface Temperature Radiometer (SLSTR).Rows highlighted in blue show bands that match with Landsat-8/OLI.

SLSTR band	L centre [µm]
S1	0.555
S2	0.659
S-3	0.865
S4	1.375
S5	1.61
S6	2.25
S7	3.74
S8	10.95
S9	12
F1	3.74
F2	10.95

Table 3: Band characteristics of Landsat-8.

Band	Wavelength (nm) range	[central]	GSD (m)	SNR at reference L	reference L (W m^{-2} sr^{-1} μm^{-1})	F0 (W m^{-2} μm^{-1})
1 (Coastal/Aerosol)	433–453	[443]	30	232	40	1895.6
2 (Blue)	450–515	[483]	30	355	40	2004.6
3 (Green)	525–600	[561]	30	296	30	1820.7
4 (Red)	630–680	[655]	30	222	22	1549.4
5 (NIR)	845–885	[865]	30	199	14	951.2
6 (SWIR 1)	1560–1660	[1609]	30	261	4	247.6
7 (SWIR 2)	2100–2300	[2201]	30	326	1.7	85.5
8 (PAN)	500–680	[591]	15	146	23	1724.0
9 (CIRRUS)	1360–1390	[1373]	30	162	6	367.0